Optics and Laser Technology 122 (2020) 105859

Contents lists available at ScienceDirect

Optics and Laser Technology

journal homepage: www.elsevier.com/locate/optlastec

Review

Terahertz phase imaging and biomedical applications

Min Wan, John J. Healy, John T. Sheridan*

School of Electrical and Electronic Engineering, IOE2 Lab, College of Architecture and Engineering, University College Dublin, Belfield, Dublin 4, Ireland

HIGHLIGHTS

- Continuous Wave (CW) and pulsed THz phase imaging systems are reviewed.
- CW techniques examined include holography, interferometry and ptychography.
- Pulsed THz techniques, including time domain holography, are discussed.
- Phase extraction methods are discussed.
- Biomedical applications of such THz systems are highlighted.

ARTICLE INFO

Keywords:
Terahertz imaging
Phase imaging
Terahertz pulsed imaging
Digital holography
Biomedical imaging

ABSTRACT

Terahertz frequency (THz) radiation lies in between the microwave and infrared ranges. While it is strongly absorbed by water, it is nonionizing and has low possibility of causing tissue damage as it involves low energy photons. Recent technological progress in developing THz instrumentation, means that commercial THz systems are being produced with improving performance which are easier to operate and more reliable. THz phase imaging, an advanced imaging technology which combines the benefits of THz and commonly used phase imaging techniques, has recently received significant attention. In this paper, the current state of such imaging systems is reviewed. This review deals with both pulsed and continuous-wave (CW) imaging systems. Pulsed THz phase imaging is a coherent measurement, which includes terahertz pulsed imaging (TPI) based on femtosecond laser and holographic imaging in the time domain, both allow phase and amplitude information of the electric field to be recorded. CW THz phase imaging is mainly based on digital holography, interferometry and ptychography. These systems can obtain the complex amplitude by capturing diffraction patterns and applying numerical reconstruction techniques. Biomedical applications of such THz systems are highlighted.

1. Introduction

The terahertz (THz) electromagnetic radiation, commonly referred to as THz waves, THz light, or T-rays, lies in the frequency range between the microwave and infrared radiation, THz emissions have frequencies ranging from 100 GHz to 10 THz, (where 1 THz = 10^{12} Hz corresponding to 4.14 meV) and correspond to wavelengths between 30 μm and 3 mm [1]. The spectrum is illustrated in Fig. 1. Such frequencies, a million times lower than those of X rays, are non-ionizing. Therefore, THz waves have attracted increased attention because of their ability to non-destructively pass through solid objects, including those made of cloth, paper, wood, plastic, and ceramics, and to produce images of the interiors of the objects. Readers may have already encountered sub-THz body security scanners at airports.

THz light is strongly absorbed by intermolecular bonds, e.g., the hydrogen bonds present in water and the N-H bonds present in proteins. This means the imaging systems are sensitive to subtle changes involving increased water content, e.g. blood flow, which can arise due to the presence of diseased tissue [2]. THz light for medical imaging, for both screening and diagnostic purposes, may become wide spread if suitable technology and procedures can be developed.

Until recently, it has proved difficult to generate THz radiation efficiently as it required bulky and expensive equipment, e.g. free electron lasers or alternatively the use of thermal sources, to produce low power broad band incoherent radiation. In comparison with visible light, THz radiation has also proved difficult to be detected as thermal detectors requires liquid helium cooled bolometers with poor noise performance. The lack of suitable sources, sensitive detectors, and other components has led to this band of the spectrum being referred to as the "THz Gap" [3]. More recently, however the potential significance of

* Corresponding author.
E-mail address: john.sheridan@ucd.ie (J.T. Sheridan).

https://doi.org/10.1016/j.optlastec.2019.105859
Received 9 July 2019; Received in revised form 2 September 2019; Accepted 17 September 2019
Available online 11 October 2019
0030-3992/

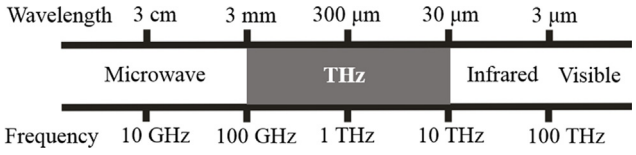

Fig. 1. The electromagnetic spectrum.

this radiation has been more fully appreciated. This has led to many new advances in the technologies for generation, manipulation, and detection of THz radiation which is revolutionizing the field. This upsurge in activity is motivated by the large number of possible applications of THz imaging, communication sensing, and spectroscopy.

Two major types of THz system sources exist: continuous-wave (CW) and time-domain spectroscopy (TDS, pulsed) systems. CW systems typically operate at a single frequency, (i.e. narrow band), with the THz source wavelength being variable or tunable. Generally, CW sources can generate higher output power (> 10 mW) than pulsed sources ($\sim\mu$W). Specific implementations included, for example, quantum cascade lasers (QCL) [4], backward-wave oscillators (BWO) [5] and optically-pumped THz lasers (OPTL) [6]. Besides the CW source discussed, tuneable CW THz emitters, consisting of a photomixer and an optical beat source, can also be used to realize compact and cost-effective systems. The optical beat sources in the commercial CW THz photomixer systems are commonly comprised of two tuneable distributed feedback laser diodes with different wavelengths [7,8]. Terahertz time domain spectroscopy (THz-TDS) systems are based on the generation and detection of pulses which are of a few picoseconds in duration. Traditionally time domain systems used femto-second lasers (such as a Ti:Sapphire mode-locked laser that produces femtosecond laser pulses with a wavelength of around 800 nm) to pump a photoconductive antenna or electro-optical crystals such as $LiTaO_3$ and ZeTe to generate the output THz pulses [9].

The ability to accurately detect THz radiation is at the heart of THz technology. For pulsed THz systems, there are two commonly employed detection methods. In the case of photoconductive sampling, systems based on an above-band-gap excitation in a semiconductor [10] are used. Typically, fast photoconductors, such as radiation-damaged silicon or low-temperature-grown GaAs are used to provide the necessary sub-picosecond sampling resolution. Some other detectors are based on free-space electro-optic sampling, in which the THz field induces birefringence in an electro-optic medium [11,12]. This birefringence is sampled using an optical probe beam as a function of the delay between the probe pulse and THz pulse. The resulting sampling resolution is determined largely by the duration of the optical probe pulse.

CW THz imaging systems provide an incoherent detection method for the THz wave. Detectors such as a bolometer or a Golay cell [13] are commonly used. Array detectors are also available for direct detection, including microbolometer arrays [14,15], germanium detector arrays [16] and pyroelectric cameras [17]. Using these different systems, a wide number of imaging methods have been proposed, including THz tomography [18,19], THz near-field imaging [20], THz focal scanning imaging [21,22], etc.

Most CW imaging methods explored only capture the intensity information of the object. However, in general, the phase information not only supplies higher imaging contrast for transparent samples, but also provide information unavailable otherwise, i.e., the relative optical depth profile of the sample's surface and interior density. To extract more information about the object, phase contrast imaging methods are critically important as they contain topographic information. Diseased tissue, when compared with normal or healthy biomedical tissue, typically contains more water [23]. Other changes arise as a result of oedema or increased vascularity. It is often difficult to evaluate tissue characteristics from intensity-based absorption characteristics alone. Therefore, phase imaging is necessary for THz biomedical applications.

We now review the potential of THz phase imaging method based on pulsed and CW THz sources. Pulsed THz imaging not only provides valuable spectral information but also two-dimensional images by scanning either the THz beam location or by moving the object itself. Both the amplitude and phase of the scattered THz field can be obtained simultaneously by recording the wave's temporal electric fields. This is discussed in more detail below in Section 2. In this part, we discussed the principle of TPI and phase unwrapping techniques in THz pulsed imaging. Meanwhile, holographic imaging in time domain is also reviewed. In Section 3, CW THz phase imaging is discussed in the context of THz digital holography (TDH), THz interferometry and THz ptychography. In Section 4, the application of THz technology to biomedical imaging is then briefly reviewed. Finally, we present our summaries.

2. Pulsed- THz phase imaging

2.1. THz pulsed imaging

THz time domain spectroscopy (TDS) is a coherent technique that provides a measurement of the THz electric field by employing short pulses of broadband THz radiation and utilizing time-delay detection. This technique can be extended to perform TPI, providing a novel, non-invasive imaging method which allows both phase and amplitude information to be extracted. TPI captures the THz time domain waveform which contains object information. The amplitude and phase of the object wavefront are obtained by calculating the Fourier transform in the frequency domain. This provides valuable spectral information, and the object location if accurate scanning is performed using a two dimensional (2D) electrical translation stage. In this way, the 2D images can be mapped out pixel by pixel by scanning either the THz beam or the object itself. The resulting image of the sample can be processed to reveal its inner structure providing three-dimensional information.

TPI systems can be used in either transmission [24] or reflection geometries [25,26], see Fig. 2(a) and (b), respectively. The incident THz radiation is either transmitted through the sample or is reflected from the sample and then detected.

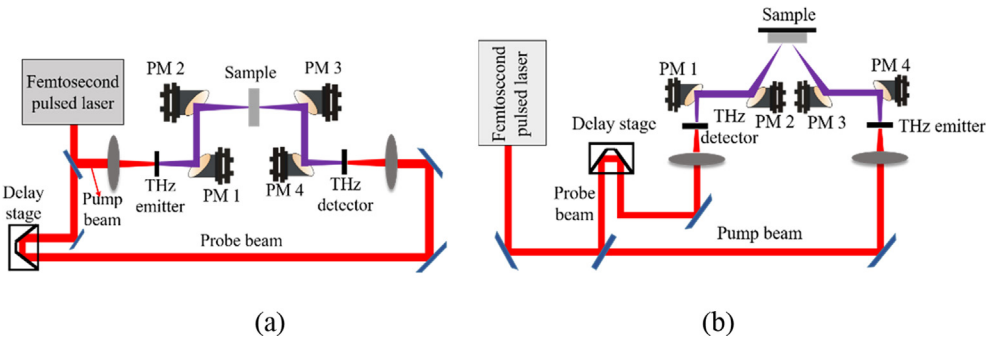

Fig. 2. Terahertz pulsed imaging for (a) transmission and (b) reflection geometries. PM, parabolic mirror.

The systems typically operate as follows: the light from pulsed femtosecond laser pumps a crystal to generate a broadband THz radiation. The scattered radiation is mapped pixel by pixel using *x-y* translation of the sample or the beam in the focal plane of frequency domain. Off-axis parabolic mirrors seen in Fig. 2 are used to focus the generated THz pulse onto the sample and to collect the reflected or transmitted pulse after interaction with the sample. This radiation is then recombined with the probe beam to interfere at the detector stage. A number of different detector techniques can then be employed, *e.g.*, bolometric measurement, electro-optic sampling [27] or a photoconductive receiver. The photoconductive receiver is typically fabricated from the same semiconductor crystal as that used to implement the photoconductive emitters. The time at which the measurement is made is determined by the time delay of the probe beam, determined by an optical delay stage. The entire THz pulse profile is reconstructed by scanning the optical delay line across the selected time-domain range and sampled at predetermined time values.

For biomedical imaging, TPI systems are typically used in a reflective geometry. This is because the biological samples, which typically contain high water contents, need to be very thin if they are to be measured in transmission geometry as THz radiation is so strongly absorbed by water. To avoid the necessity of performing complex sample manipulations prior to imaging [26], the reflection geometry is most feasible. In that case, as the samples do not need to be thin, TPI can be performed in a clinical setting.

Phase unwrapping technique plays an important role in phase imaging. Following processing, the wrapped phase maps extracted contain discontinuities as the phase front contains phase shifts greater than 2π rad for objects causing optical phase shifts corresponding to optical path lengths greater than imaging wavelength. Most phase-unwrapping algorithms [28,29] require the use of a priori information to avoid such ambiguity. A synthetic wavelength approach was applied by Zhang et al. in 2006 [30] to solve phase unwrapping problem. Two separate wavelengths λ_1 and λ_2 are used related to two phase images φ_1 and φ_2, given a surface profile $d = \lambda\varphi/2\pi$. The experimental apparatus is shown in Fig. 3. Pumping is performed using a femtosecond pulse laser with 810 nm central wavelength and 100 fs pulse duration. The laser pulse is split into a pump beam and a probe beam passing through a half wave plate. An InAs crystal was used to generate terahertz pulses. The object placed in the focal plane of the second off-axis parabolic mirror. This object can be moved in the *x-y* plane. The THz pulses were focused on a ZnTe crystal. The probe beam also focused on to the same spot on the ZnTe crystal. The THz wave incident on the crystal modulate the polarization of the probe beam via the electro-optic effect inside the ZnTe crystal. A photodetector was used to measure the intensity. Two wavelengths, 0.30 mm (1.0 THz) and 0.27 mm (1.1 THz) provided a synthesized wavelength of 2.7 mm.

An example of the results produced using such of dual-wavelength phase images was published in [30], an object with a groove has been imaged which has 9 mm depth and 10.4 mm width. The results show the exact profile of the groove. Using a standard phase-unwrapping algorithm, the phase images corresponding two single-wavelength at the frequencies of $f_1 = 1.0$ THz and $f_2 = 1.1$ THz are processed, respectively. The results of dual-wavelength image of the groove are much smoother and less noisy. THz reflective focal-plane multi-wavelength phase imaging was implemented by the same group in 2009 [22]. A Spectra Physics Hurricane with 1 kHz repetition rate was used as pulsed laser with 75 fs pulse duration and 795 nm center wavelength. A metallic washer was used as the sample to be inspected and the reconstructed phase image was clearly illustrating this method. The frequency range used was limited to be between 0.4 THz and 1.0 THz. The corresponding resulting of phase image are obtained respectively single wavelength at 1.0 THz and multiwavelength. This method has 300 μm resolution and can be used to resolve fine details in the object.

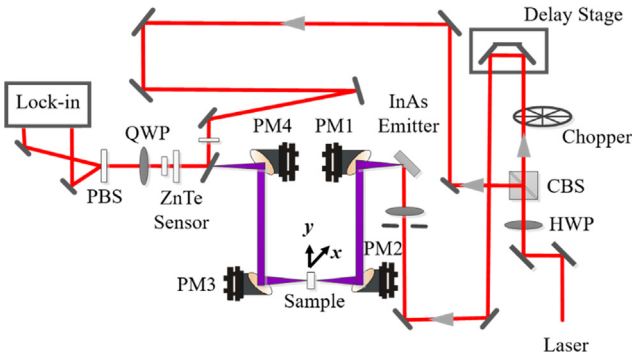

Fig. 3. THz dual-wavelength time domain phase imaging experimental apparatus. CBS, cubic beam splitter; HWP, half-wave plate; PM, parabolic mirror; QWP, quarter-wave plate; PBS, polarizing beam splitter.

2.2. Holographic imaging in the time domain

In 2000, Ruffin *et al.* [31] demonstrated time reversal imaging that can be considered THz holographic imaging in the time domain. In 2008, pulsed THz digital holography was investigated by Zhang *et al.* [32]. This is another terahertz time domain phase imaging method. An experiment setup is shown in Fig. 4. Samples were illuminated by a Gaussian profile THz beam and the transmitted waves were reflected towards a ZnTe electro-optics (EO) crystal by an indium tin oxide (ITO) THz mirror. Note that the transmitted optical probe beam propagated collinearly with the THz beam. Once again, the ZnTe EO crystal modulated the polarization of the probe beam via the EO effect [11]. Therefore, the THz diffraction pattern was encoded onto the probe beam by changing the time delay with respect to the probe. The probe beam was imaged by the lens onto the imaged CCD. The spatiotemporal distribution of a THz hologram was obtained by using a metallic cross as the object. The reconstructed image was retrieved using the angular spectrum algorithm to model the propagation of the THz pulse in free space.

In 2012, a metallic coaxial waveguide was characterized using a pulsed THz digital holography system [33]. A numerical implementation of the inverse Fresnel diffraction algorithm was then used to successfully reconstruct the waveguide mode patterns. A converging spherical field undergoes an axial phase shift in passing through the focal point, this is Gouy phase shift [34–36]. In 2013, the properties of the Gouy phase shift in a converging THz spherical beam was observed using a pulsed THz holographic system operating in the time domain [36]. Applying this pulsed THz digital holographic system, THz vortices [37,38], meta-materials [39] and Bessel beams [40] have been investigated.

In 2017, the natural dehydration processes of three types of biological tissues were observed [41] employing a pulsed THz digital holographic imaging system. A diagram of the experimental setup is given in Fig. 5. The femtosecond laser pulse with 800 nm central wavelength is split into the pump beam and the probe beam for exciting and probing

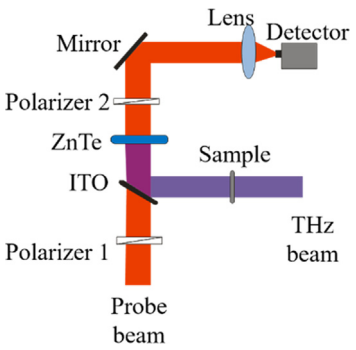

Fig. 4. The schematic illustration of THz digital holography in the time domain.

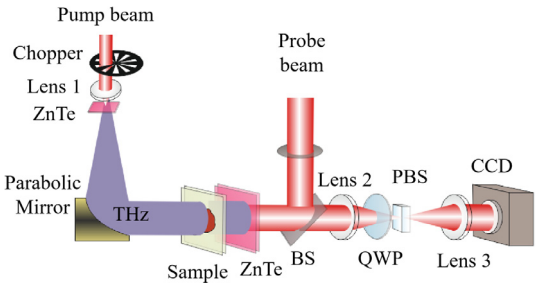

Fig. 5. Schematic diagram of a THz digital holographic imaging system based on femtosecond laser pulse.

the THz radiation. A ZnTe crystal was used radiate THz waves via the non-linear optical rectification. The sample was then illuminated by the THz beam. The transmitted THz beam with sample information was modulated on the polarization state of the probe beam by another detection ZnTe crystal. The probe beam was measured by a CCD camera. The THz images in the time domain were abstained by adjusting the optical path difference between the probe beam and the THz beam. The angular spectrum algorithm was applied to perform image reconstruction. This further work broadens the potential of this imaging method for biological application. Since pulsed THz imaging has been study for decades, more updates related with pulsed THz imaging can be found in Ref. [42].

3. CW-THz phase imaging

In spite of the excellent properties of pulsed THz phase imaging, the requirement to use a femtosecond laser considerably increases the cost and complexity of such systems. Furthermore, such systems can only operate stably under conditions of precise temperature and humidity control. In addition, most of the THz sources available which require the use of femtosecond pulses do not provide high intensities, severely limit the resulting range of THz imaging applications. With the emergency of new generation THz sources [43,44], detectors [45,46] and imaging components, it has provided an alternative approach to avoid the drawbacks associated with pulsed THz systems. CW systems can provide stable output intensity and can be made immune to variations in temperature and vibrations. Since such system do not require a pump–probe geometry and require less optical components compared to pulsed THz systems, image acquisition would be faster. Employing phase sensitive detectors and high-power CW terahertz sources, continuous-wave terahertz digital holography (TDH), interferometry and THz ptychography are proposed. Depending on different method and system used to produce the various types of CW THz phase imaging, a year ordered flow chart is shown in Table 1. Some of the methods used will now be discussed in more detail.

3.1. CW-THz digital holography

Holography [47], has been employed as a valuable phase imaging tools for characterization and diagnostics in many technical fields. The holograms are typically recorded by capturing the interference pattern of the field scattered by the object and a known reference wave. Reconstruction of the hologram, involving Fourier scalar diffraction theory, enables information to be extracted from the captured three-dimensional image data. For digital holography in visible light domain, the hologram is recorded using a CCD/CMOS camera [48]. Once the hologram has been recorded, numerical methods can be adopted to reconstruct the optical field. Some processing techniques are Huygens convolution, the Fresnel transform, and angular spectrum methods [49]. Compared with traditional optical holography, digital holography has many practical advantages, e.g., real time imaging, non-destructive phase contrast imaging. CW THz digital holography combines the advantages of THz radiation and digital holography. Various configurations are now discussed. Depending on the angle between the reference and object beams, CW TDH can be divided into in-line [50,51] and off-axis geometries [52–54]. Off-axis TDH can be used for both reflective and transmission imaging to perform general surface morphology. The feasibility of TDH based on CW source was revealed by Mahon *et al.* in 2006 [55]. The resulting Fresnel off-axis digital holographic setup which employed a 100 GHz Gunn diode with 35 mW output as the CW THz source, a Schottky-barrier diode as the scanning detector, is shown in Fig. 6. A 3 dB cross-guide coupler was used to split the THz beam into two beams of equal power. A slightly irregular "M" shaped mask, having a minimum structure size of 9 mm, was used as the object sample. The hologram quality is defined by the interference pattern. Neglecting detector (e.g. SNR) and environmental (e.g. vibration) limitations on the measurement, sharp stable fringes, having maximum contrast, can be best obtained using a coherent narrow band THz source and appropriately adjusting attenuators situated in the interfering beams (typically in the reference arm).

Point scanning imaging however is limited by the time-consuming mechanical scanning thus cannot provide real-time two-dimensional imaging. The development of array detectors provide the opportunity to achieve higher speed of data acquisition. Attempts have therefore been made to implement CW TDH using array detectors [52,53].

Cherkassky *et al.* in 2010 studied THz Gabor in-line digital holography using a tunable THz free electron laser working at wavelengths of 130 μm and 68 μm [56,57]. An InAs NIR thermograph and CCD array detector were used to record the holograms, but the reconstructed images were not very clear. In 2011, a series of THz digital off-axis holographic system was implemented by Li *et al.* using a SI-FIR-50 far-IR gas laser operating at a frequency of 2.52 THz and having 50 mW output [53]. A commercial pyroelectric array camera, Pyrocam III, from Ophir-Spiricon, Inc. [17], was used to capture images. The array had 124 × 124 pixels of size 85 μm × 85 μm, and element spacing of 100 μm × 100 μm, so the active area was 12.4 mm × 12.4 mm. The experimental setup is shown in Fig. 7. It was found that the hologram quality was degraded by speckle noise and diffraction effects. The zero-order diffraction contained most energy for off-axis DH. To suppress noise, averaging over ten sequential frames captured by the camera was used to produce much improved holograms. Numerical reconstruction was performed using a Laplacian-filter algorithm which performed filtering in the frequency domain. The image resolution of the reconstructed real images was better than 0.4 mm.

In 2012, phase retrieval was employed to perform THz holographic imaging at 310 GHz by Enayati *et al.* [58]. A CW THz radiation at 310 GHz was used to illuminate the object. A heterodyne receiver in the x-y plane was used to measure the complex field. In this case, the object was a 10 cm × 10 cm aluminium rectangle containing holes and slots. The strong gradients localized at the edges in the reconstructed image confirmed the validity of the approach. This method can be employed to improve the image quality of holographic imaging systems at other frequency. In 2014, Hack *et al.* measured both the amplitude and phase of an object using a transmission geometry off-axis holographic system implemented with a 3 THz Quantum Cascade Laser with 1.2 mW peak power and an array detector [59]. The detector was a micro-bolometer array with 640 × 480 pixels on a pitch of 25 μm. The Fresnel-Kirchhoff back propagation algorithm was used to reconstruct the complex object image. A lateral resolution of 280 μm and a relative phase sensitivity of about 0.5 rad were estimated based on the reconstructed images of a metallic Siemens star and a polypropylene test structure. In 2015, THz digital holography was applied to image dielectrics, which were opaque in the visible, by Heimbeck *et al.* [60]. A THz off-axis holography system was implemented using a multiplier chain driven by a 10–20 GHz microwave synthesizer from Virginia Diodes, Inc. (VDI) [61] as the THz source. A raster scanning heterodyne detector was used instead of a Schottky diode detector to acquire a hologram. The samples inspected were 3D printed dielectric masks, one of which contained a

Table 1
Overview of systems for CW THz phase imaging.

Type	Name	Method	Source	Detector	Instruments
CW THz interferometry	Lu *et al.* in 2008 [86,87]	Subwavelength plastic fiber-based THz endoscope	320 GHz Gunn oscillator	Golay cell detector	Fabry Perot interferometers
	Wang *et al.* in 2010 [82]	CW THz multi-wavelength method	0.10 THz Gunn diode and 0.12 THz backward wave oscillator	Pyroelectric detector	Michelson interferometer
	Wang *et al.* in 2011 [83]	An improved four-step phase shifting algorithm	2.52 THz CPTL	Golay cell detector	Michelson interferometer
	Sun *et al.* in 2013 [85]	Three step phase shifting algorithm	0.39 THz Gunn diode	Schottky diode	Michelson interferometer
CW off-axis transmission TDH	Mahon *et al.* in 2006 [55]	Proposed TDH	100 GHz Gunn diode	Schottky diode	Fresnel off-axis TDH
	Heimbeck *et al.* in 2011 [78]	Dual wavelength reconstruction methods	0.66–0.76 THz tunable CW source	Schottky diode	Mach-Zehnder interferometer
	Li *et al.* in 2011 [53]	Proposed off-axis TDH using array detector to record hologram	2.52 THz CPTL	Pyroelectric array detector	Off-axis TDH
	Li *et al.* in 2012 [66]	Reduce recording distance, zero-order diffraction suppression method.	2.52 THz CPTL	Pyroelectric array detector	Off-axis TDH
	Li *et al.* in 2012 [67]	Three different numerical algorithms for reconstruction	2.52 THz CPTL	Pyroelectric array detector	Off-axis TDH
	Yuasa *et al.* in 2013 [80]	THz computed tomography	Frequency multiplier with 540 GHz	Schottky diodes	Mach-Zehnder interferometer
	Hack *et al.* in 2014 [59]	Image plane holography	3 THz QCL	Micro-bolometer array detector	Off-axis TDH
	Locatelli *et al.* in 2015 [81]	THz DH real-time imaging	2.8 THz QCL	Micro-bolometers array detector	Mach-Zehnder off-axis system
	Heimbeck *et al.* in 2015 [60]	Voids imaging within visually opaque dielectrics	0.495 THz and 0.710 THz multiplier chain	Schottky diode	Off-axis TDH
CW off-axis reflection TDH	Enayati *et al.* in 2012 [58]	Phase retrieval method in TDH at 310 GHz	310 GHz Coherent transmitter	Heterodyne receiver	Off-axis TDH
	Zolliker *et al.* in 2015 [52]	Synthetic aperture method 1.68λ (200 μm)	2.52 THz CPTL	Micro-bolometer array detector	Off-axis TDH
	Hack *et al.* in 2017 [63]	Topography of concealed object under opaque materials	2.52 THz CPTL	Micro-bolometer array detector	Off-axis TDH
	Wang *et al.* in 2019 [75]	Subpixel image registration and image fusion algorithms to expand FOV of the system	2.52 THz CPTL	Pyroelectric array detector	Off-axis TDH
CW in-line TDH	Cherkassky *et al.* in 2010 [56,57]	In-line DH	THz free electron laser	InAs NIR thermograph & CCD	In-line TDH
	Li *et al.* in 2012 [51]	Proposed in-line TDH using array detector to record hologram	2.52 THz CPTL	Pyroelectric array detector	In-line TDH
	Li *et al.* in 2014 [68]	Comparison of phase retrieval algorithm	2.52 THz CPTL	Pyroelectric array detector	In-line TDH
	Rong *et al.* in 2014, [50]	The extrapolation method.	2.52 THz CPTL	Pyroelectric array detector	In-line TDH
	Huang *et al.* in 2016 [74]	Synthetic aperture, resolution 1.28λ (125 μm)	3 THz QCL	Micro-bolometer array detector	In-line TDH
	Huang *et al.* in 2017 [69]	Autofocusing method with phase retrieval in TDH	2.52 THz CPTL	Pyroelectric array detector	In-line TDH
CW THz ptychography	Hack *et al.* in 2018 [92]	Demonstration this system	3.1 THz CW laser	Micro-bolometer array detector	Ptychography
	Rong *et al.* in 2019 [93]	Probe position correction, first biological imaging	2.52 THz CPTL	Pyroelectric array detector	Ptychography

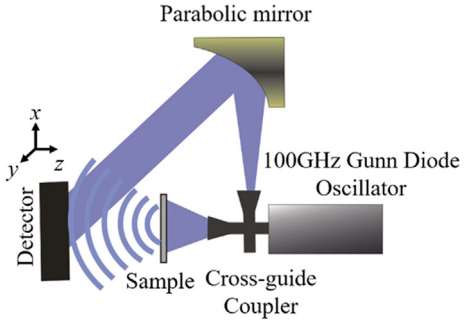

Fig. 6. Experimental arrangement for the creation of THz digital holograms.

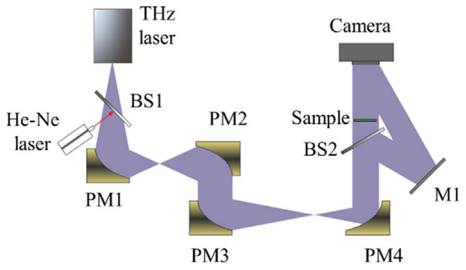

Fig. 7. Transmission geometry of off-axis holographic system.

variety of absorbent-filled void structures having slightly different dielectric constants. Another sample contained arrays of empty square voids of increasing depth which induced Fabry–Pérot cavity effects. The object was a dielectric transmissive and absorptive resolution chart. To enhance the resolution, the hologram was recorded at a distance of 163 mm from the sample so as to minimize the sample to detector distance. More than 24 h was needed to capture the data, composed of 1000 × 1000 individual measurements separated by a 0.2-mm scanning steps size. Reconstructed results at frequency of 0.495 THz and 0.710 THz were demonstrated using the angular spectrum method. The image resolution was calculated applying the Rayleigh criterion and voids as thin as 45 μm were successfully observed. This corresponding to $\lambda/13$ and $\lambda/9$ for the 0.495 THz and 0.710 THz images, respectively.

In 2016, Hack *et al.* compared the imaging properties of four different array detectors. The effects of using different beam profiles, relative camera responses and interference patterns were studied in each of the four cases [62]. In 2017, using a digital holographic setup, a method for signal separation was demonstrated which can retrieve the amplitude and phase distributions of the radiation scattered from a covered object embedded behind an opaque material [63]. The principle of using a three-beam interference method was theoretically analyzed and the system performance illustrated by simulation. The covered sample used in the experiments was a 2 mm thick Teflon (PTFE) plate which is highly transparent and weakly scattering in the THz range but completely opaque to visible light. In the same year, Yasui *et al.* reported an off-axis terahertz digital holography system employing a 3 THz quantum cascade laser and a micro-bolometer array in which the amplitude and phase images were reconstructed from the recorded holograms using the angular spectrum algorithm [64].

Imaging resolution is one of the key parameters in determining the quality of a reconstructed wavefront in digital holography. When array detection is used, resolution and fidelity enhancement methods have been independently applied by several research groups. The resolution of such CW TDH is ultimately determined by the ability of the system to capture the high-frequency components containing the fine details of a sample. During the propagation from object to the detector, the high spatial frequency component of the field propagates with larger diffraction angles. Such wave components may walk away, and not impinge on the array, in which case the interference fringes at the recording plane may not overlap on the sensitive detector area. The finite number and the size of recording pixels in the detector array also limits the resolving power of the holographic system due to the loss of high-frequency components. Therefore, the lateral resolution is limited by: (a) the numerical aperture of the system and (b) the sensor pitch. In-line THz digital holography system implementations can provide higher resolution than the equivalent off-axis implementation. The Gabor in-line scheme does not require an additional reference beam, and the lateral resolution is only limited by the systems numerical aperture. In addition, in-line digital holography has significantly lower requirements for the coherence of the THz source, which reduces the energy loss and distortion during propagation. Further refinements are continually being proposed to provide resolution enhancement for CW TDH.

The physical parameters in THz digital holography are significantly different from those involved in visible light digital holography. For example, the size of THz digital holograms and the recording distance used are typically of the same order of magnitude. For such values, the Fresnel approximation conditions are not well satisfied. The diffraction effects are much more significant in terahertz domain than for visible wavelengths.

In 2012, Li et al. used the system studied in [51] for in-line TDH, see Fig. 8. In such systems, the lateral resolution can be improved by reducing the recording distance between the object and the detector. For a fixed object of a certain size, a minimum recording distance exists for the system. The convolution reconstruction algorithm was used for reconstruction and the system achieved a resolution of 0.2 mm. This system was also shown to be capable of imaging concealed objects [65]. To improve imaging quality of off-axis TDH, it was reported that (a) the recording distance could be further reduced and (b) zero-order diffraction suppression methods can be used [66].

The recording and numerical reconstruction processes for CW TDH was also discussed by Li *et al.* in 2012 [67]. The reconstruction performance of the Fresnel angular spectrum algorithm, the Rayleigh–Sommerfeld convolution algorithm and the angular spectrum algorithm were compared. The results of numerical simulation and experiment were compared and analyzed using a 2.52 THz off–axis CW TDH imaging system. It is essential to choose the optimal algorithm in the reconstruction progress to quantitatively determine the actual experimental improvements. Iterative phase retrieval algorithms can be used to obtain the phase distribution from the intensity distribution (holograms) in an in-line holographic set-up. In THz in-line digital holography, the reconstructed image quality is degraded by the presence of the zero-order diffraction light and conjugate images. In 2014, three different phase retrieval algorithms [68] were applied to reconstruct complex objects applying the diffraction propagator, the object plane and the image plane constraints. The effects of numerical techniques, such as zero padding and boundary replication expansion, were also studied. It has been shown that the conjugate image present in in-line holography can be greatly reduced by adopting an appropriate phase retrieval algorithm. The accuracy of the value of the

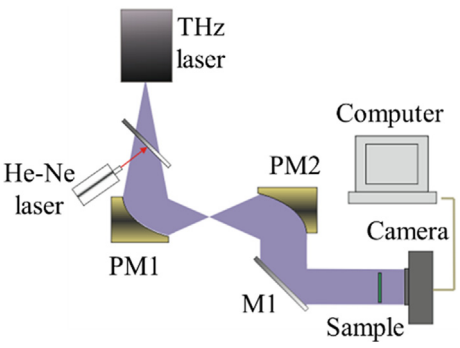

Fig. 8. The geometry in-line CW TDH system.

propagation distance used is key during reconstruction as it is necessary in order to extract the object information accurately. The use of an accurate autofocusing algorithm, in conjunction with the phase retrieval method, was introduced to automatically determine the propagation distance [69]. Autofocusing was also used in multi-plane THz imaging for in-line digital holography in 2017 [70].

The synthetic aperture method, which seeks to increase the numerical aperture, has been demonstrated to be an effective way to improve the resolution of TDH [71–73]. In 2015, Zolliker *et al.* implemented a THz synthetic aperture system to enhance the resolution [52]. A reflection geometry TDH geometry was shown suitable for samples with considerable absorption. The source used was a far infrared laser FIRL100 (Edinburgh Instruments) with a CW power of up to 150 mW, the detector was again employed a micro-bolometer array same as in [59]. The targets used included a Siemens star with an outer diameter of 12 mm, a stainless-steel disk and a Swiss five cent coin. The image reconstruction method used the fast Fourier transform with a special transformation to handle tilts and offsets of planes. The complex field of the object was retrieved by two steps: First, the field was backpropagated to a plane parallel to the detector plane. Second, the field was propagated to a tilted plane with a specific angle. To increase the lateral resolution, a synthetic aperture method was used to increase the numerical aperture in TDH. The fused hologram was synthesized by stitching 19 overlapping frames. A lateral resolution of 200 μm and a relative phase sensitivity of ~ 0.4 rad, corresponding to a depth resolution of 6 μm, was demonstrated using two specially prepared test targets. The results indicate that TDH has a practical potential for surface profilometry. In 2016, Huang *et al.* implemented a synthetic aperture method in transmission type in-line digital holographic architecture [74]. A quantum cascade laser (QCL) was adopted, emitting CW THz waves at 97, 97.6, and 98.9 μm simultaneously, with a power ratio of 4:1:2, respectively. The digital holograms were captured by an uncooled microbolometer detector (*NEC Corp*) with 320 × 240 pixels and 23.5 μm × 23.5 μm pixel pitch. In order to record the expanded hologram, this detector was mounted on a 2D translation stage. Stripe resolution charts were used to verify the system resolution and resolution of 125 μm was demonstrated. Because the sample was illuminated by a finite collimated beam, the size of the hologram was constrained by the extent of the unscattered reference beam, i.e, the resolution enhancement of this method is limited. In 2019, Wang *et al.* applied subpixel image registration and image fusion algorithms to expand the field-of view (FOV) of a CW THz reflective digital holography [75]. The amplitude and profile distributions of a covered object was measured. The system FOV was expanded 1.75 times compared with a reconstruction results achieved employing a single hologram.

A computational resolution improvement method, the extrapolation method, involves posteriori increasing the detector size, i.e. the system numerical aperture (N.A.), and has been applied to in-line THz holography by Rong *et al.* [50,76]. The extrapolation procedure is described in detail in [77] involving a modified padding of the hologram. Like mainstream phase retrieval algorithms for in-line holograms, the positive absorption constraint is used in the object plane in this method. After propagating to the recording plane, the amplitude of the area covering the original hologram is updated by the square root of the recording intensity, while the amplitude of the expanded area is kept the same as the phase distribution in that plane. The high frequency component of the object wave beyond the aperture of the hologram is numerically retrieved after iterations. To increase the signal-to-noise ratio for in-line THz hologram and background images, a Gaussian fitting method is proposed. The source used was a FIRL100 THz laser operating at 2.52 THz having 150 mW output power. A pyroelectric array detector (Pyrocam III) with 12.4 × 12.4 mm total active area, was used to record the holograms. The extrapolation procedure increased the effective size of the hologram from 12.4 mm × 12.4 mm to approximately 33.0 mm × 33.0 mm. In this way, the theoretical resolution was predicted to improve from 164.4 μm to 82.8 μm according to the Abbe criterion. In Ref. [50], CW THz digital holography was adopted for biological imaging. The sample examined was a dragonfly hindwing which contains features such as widths of the costa, radius vein, median veins and cross veins having size of approximately 110 μm, 70 μm, 35–48 μm, and 33–40 μm, respectively. Using iterative reconstruction with extrapolation, the smallest feature resolved in the reconstruction progress was cross veins.

3.2. THz interferometry

Interferometers are popular metrological tools used in many fields of science and engineering. They work by merging two or more coherent light sources to create an interference pattern, which can be measured and analyzed. The interference patterns generated contain information about the object being studied. Interferometrical techniques naturally complement holographic, multi-wavelength methods to produce surface contours and deformation measurement. Interferometry is a classical phase-measurement technique. However, most interferometers are used in the visible light domain. With THz technology development, a range of different interferometers have been applied in the THz band.

In 2011, Heimbeck *et al.* demonstrated terahertz digital off-axis holography using a Mach-Zehnder interferometer [78]. A coherent tunable CW THz source was (0.66–0.76 THz) implemented using a microwave synthesizer and multiplier chain of four frequency doublers and one tripler. A single, spatially-scanned Schottky diode was used for detection. The THz radiation was collimated by an off-axis parabolic mirror and divided into the illumination beam and the reference beam using a beam splitter. The object was illuminated in transmission mode and a second beam splitter was then used to recombine the scattered object beam and reference beam. The fringes were recorded in the detector plane. The experimental setup is shown in Fig. 9. The holograms were captured at 680.0 and 725.0 GHz, corresponding to wavelengths of $\lambda_1 = 0.4418$ mm and $\lambda_2 = 0.4438$ mm. Dual-wavelength phase unwrapping approach was used to overcome the 2π phase ambiguity and improve the image quality [79]. The axial resolution was about 10 μm ($\lambda/40$ at 725 GHz) when a 0.2 mm scan steps was used. The angular spectrum method was applied, in conjunction with Fourier filtering, to suppress the twin image and DC term in the reconstruction images (amplitude and phase). The precise phase image was obtained using dual-wavelength phase unwrapping. In 2013, a THz computed tomography (CT) method based on phase contrast using a Mach-Zehnder interferometer was proposed by Yuasa *et al.* The phase shift information is retrieved at each data point through a phase modulation technique employing a 0.54 THz CW source and a Schottky-barrier diodes detector [80]. A polystyrene foam sphere of 30 mm diameter having two channels of 5 mm in diameter was imaged. 5 mm (9λ) resolution was in this way achieved.

A Mach-Zehnder off-axis geometry of TDH system was reported by Locatelli et al. in 2015 [81]. Compared with Ref. [78], this setup was implemented using a quantum cascade laser operating at 2.8 THz with 4 mW output. A micro-bolometric detector array, composed of 640 × 480 pixels having a pixel pitch of 25 μm × 25 μm, was used. The ability to record and reconstruct THz digital holograms (of both static

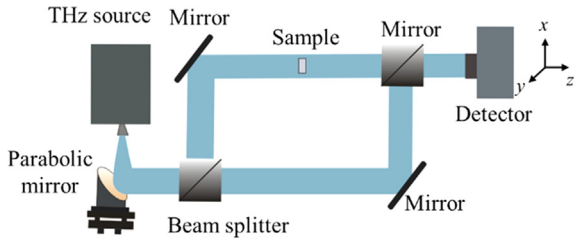

Fig. 9. THz experimental arrangement for THz Mach-Zehnder interferometer.

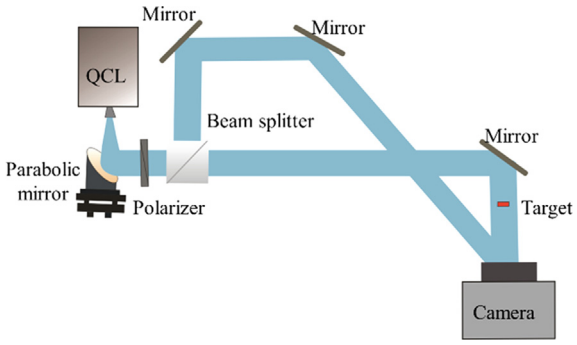

Fig. 10. Sketch of the THz DH real-time imaging experimental setup.

and dynamic scattering objects) was demonstrated using: (1) a 30 μm thick histological blank slice of healthy human skin; (2) a 1-mm thick black polypropylene sheet and (3) a 50 Lire Italian coin. The effectiveness of the proposed system for biological sample and morphology was evaluated. The experiment setup is shown in Fig. 10. In order to obtain high contrast fringes, the relative intensity ratio of the two beams was tuned using a THz wire grid polarizer positioned before the beam splitter. The reconstruction was numerically performed by Fresnel diffraction integral method. To improving the quality of the reconstructed images, the image retrieval procedure includes: (1) zero order diffraction suppression; (2) speckle noise reduction; (3) a Gaussian apodization mask to reduce the low frequency noise; (4) zero padding and the phase unwrapping method were adopted. The amplitude and phase images of healthy human skin were then extracted. Real time hologram reconstruction was numerically performed by backward propagation using the Fresnel diffraction integral.

One common configuration for optical interferometry, the Michelson interferometer, has also been investigated for CW THz phase imaging [82,83]. Wang *et al.* presented a CW THz multi-wavelength method to reduce phase wrapping artefacts in 2010 [82]. This method had previously been used for THz pulse imaging [22], however, the phase noise was worse because the CW THz radiation has a long coherence length. The Michelson interferometer, shown in Fig. 11, was implemented using a 0.10 THz Gunn diode and a 0.12 THz BWO. Their bandwidths are givens as 1.0 GHz with 4.94 mW and 4.67 mW output power, respectively. The two THz beams were collocated by a silicon wafer beam splitter (BS 1). The beams were split into a reference beam and an object beam by another silicon wafer (BS 2). The object wave was focused on the sample surface by lens (L3) and mirror M2 mounted on computer-controlled stages: linear Stage 1 and Stage 2. The sample could be scanned in one direction by the linear Stage 3. Both reflected transmission and reference waves were focused by lens L4 on to the detector. A pyroelectric detector was used to measure the interference pattern at each point on the sample by scanning the reference wave. In this way, the phase images at both wavelengths can be obtained simultaneously. A high-density polyethylene lens was used as an object. Applying a noise suppression algorithm and this scanning method, the lens phase profiles were accurately extracted. However, this method is time-consuming because the interference waveform needs to be scanned over each point of the sample and the imaging system itself is complicated. Furthermore, this CW system operated in the sub-millimeter region (below 1 THz), which limits the lateral resolution and depth sensitivity.

Phase shifting interferometry (PSI) has long been successfully used to accurately measure the phase profile of the samples in the visible light domain [84]. THz interferometric imaging and phase shifting technique were combined to retrieve the phase map. In 2011, in order to extend the method in [82], a far-infrared laser imaging system was implemented with a 2.52 THz (118.8 μm), 150 mW laser and a Golay cell detector [83]. An improved four-step phase shifting algorithm was implemented in this system. Depth profiles, having lateral resolutions down to 200 μm (5–7 μm depth standard deviation) of two-dimensional object, were successfully extracted with approximately 10 pixels per second imaging speed. However, this method cannot measure object depth greater than an optical path difference of one wavelength between the reference and object beams. In 2013, this work on CW THz phase imaging was extended using three-step phase-shifting algorithm and different THz sources and detectors [85]. In this case, THz source was a 0.39 THz Gunn diode with an output power of 4 mW and a bandwidth of 20 GHz, while detector used was a Schottky diode. To demonstrate the phase imaging ability of the system, two objects were measured having different thicknesses and material compositions. The system longitudinal resolution was founded to be 16.4 μm. Compared to the previous far-infrared laser imaging system [83], this system had a longer synthetic wavelength due to Gunn diode employed. The experimental results for multi-wavelength and three-step phase-shifting imaging were compared. Three-step phase-shifting had significantly better imaging quality and shorter acquisition times were needed.

The use of Fabry Perot interferometers in the THz was investigated using subwavelength plastic fiber-based THz endoscope by Lu et al. in 2008 [86,87]. A reflective CW THz imaging system was implemented using a Gunn oscillator module with the frequency of 320 GHz and 350 μW output power and a Golay cell as detector, see Fig. 12. Two THz sub-wavelength plastic fibers, the input fiber (dot line) and the imaging fiber (solid line), were used to form a fiber-based direction coupler. THz sub-wavelength polyethylene (PE) fibers with 240 μm diameter were used. The THz wave from Gunn oscillator was coupled into the input fiber. A fraction of this input power coupled into the imaging fiber because the two fibers were parallel and touched each other forming a directional coupler between two polyethylene (PE) films. There was a small hole on two PE films for holding the two overlapped fibers together. The angles of the input and output fiber (see Fig. 12) were θ_1 (~7°) and θ_2 (~37°). In this case 20% of the incident THz power illuminated the object. The coupled THz wave illuminated the sample which was mounted on a two-dimensional motion stage. The reflected radiation from the sample was coupled back into the imaging fiber and returned to the Golay cell for detection. In this system, the Fabry Perot

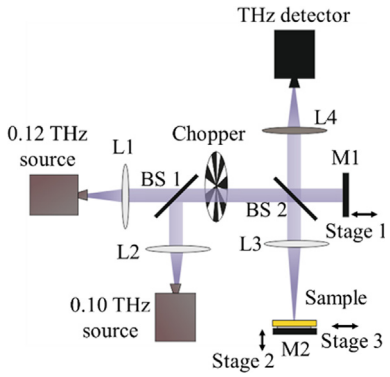

Fig. 11. THz Experimental arrangement for the creation of Michelson interferometer.

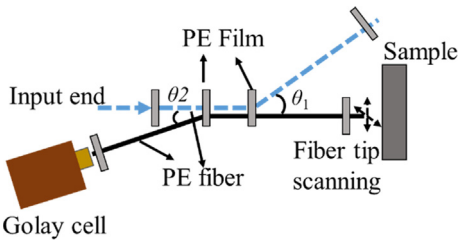

Fig. 12. THz Experimental arrangement for the creation of Fabry Perot interferometer.

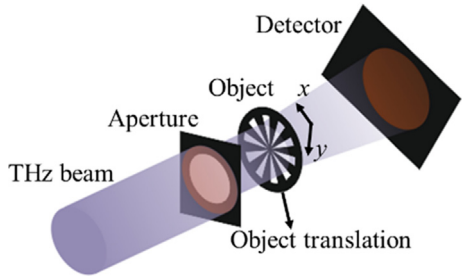

Fig. 13. THz Transmission ptychography setup.

interference occurred between the field reflected from the sample surface and the output end of the fiber. The 3D surface profiles were acquired by analyzing the THz reflection signals for different sample axial positions *x, y* and *z*.

3.3. THz ptychography

Ptychography is a non-holographic solution of the phase estimation problem., which does not need a reference beam or a lens. This method can calculate phase relationships between different parts of scattered wave with a defined coherent beam illumination, when only the magnitude (intensity or flux) of the wave can be physically measured. This phase retrieval technique was originally proposed by Hoppe et al. in the late sixties. Owing to its lensless nature, it has been particularly used in x-ray [88,89] and visible [90,91] imaging as a potential improvement on conventional coherent diffraction imaging.

In 2018, Terahertz ptychography has demonstrated by Hack *et al.* using a 3.1 THz far-infrared gas CW laser operating at $\lambda = 96.5\,\mu m$ [92]. The THz transmission ptychography system is shown in Fig. 13. The intensity of the transmission diffraction of the object is recorded by a 2D array detector with 480 × 640 pixels on a 17 μm pixel pitch (Gobi-640-GigE). THz beam was cropped by a 3 mm circular aperture to generate a probe beam before it impinged on the object. The object was shifted in the *x-y* plane until the whole object was scanned. Two types of objects, an amplitude object and a phase object were used for verifying this method. The amplitude object was a 100-μm-thick metallic nine-spoked Siemens Star. The phase object was a 2-mm-thick polypropylene (PP) slab having three different depth intersecting rings of 2.1 mm outer diameter and 1.5 mm inner diameter. After the ptychographic dataset was acquired, an extended ptychographic iterative engine (ePIE) proposed by Maiden and Rodenburg [93] was used to reconstruct the objects. The lateral resolution was less than 2λ and the depth variations was less than $\lambda/30$.

When the object is mounted on a translation stage during data acquisition, it would degrade the reconstruction quality, e.g. because of defocus, spherical aberration and position errors. In 2019, a probe position correction method that can be used for CW terahertz ptychography to improve the reconstruction was proposed by Rong *et al.* [94]. The probe positions map can be plotted by calculating the offset of the neighboring probe positions through cross-correlation registration on overlapped regions of the wave front. The simulation and experimental results demonstrated that significant reconstruction accuracy improvements are achievable. Meanwhile, Hack *et al.* proposed a coherent imaging technique which can be employed as an alternative to ptychography. The THz single-beam multiple-intensity reconstruction (SBMIR) phase retrieval algorithm simultaneously reconstructs a cover object and one hidden behind it in transmission geometry [95].

4. Biomedical applications

Since it provides many exciting new imaging modalities, THz phase imaging is rapidly being applied for: (a) biomedical use [96–98]; (b) food quality control [99–101]; and (c) metrology/morphology [52,81]. In this section, biomedical applications will be briefly reviewed.

Water content and distribution in bio-tissues is an important factor in determining and monitoring biological function. It can not only be associated with the differences between healthy and diseased tissues but also be used to identify the locations of fat and muscle. THz radiation is a viable tool for water content measurement due to its highly sensitivity to water content. In 2010, Wang *et al.* theoretically analyzed the errors in estimating water concentrations in biological tissues [102]. Using THz radiation, a coherent tunable THz source (between 0.9 and 2.5 THz) and a 4.2-K Si bolometer was used to verify the theoretical predictions. To acquire reliable results, oleic acid was used to cover (seal) the tissue samples. The imaging system itself was enclosed in a sealed box and dry nitrogen was used to suppress the absorption introduced by water vapor. In these ways, the water content and sample thickness were controlled during the experiments. For a particular THz transmittance, the accuracy of the estimated value of volume concentration of water in the tissue, *i.e.* v_w, is determined by the experimental error in the value of sample thickness *d*. This can be expressed as

$$\Delta v_w = \left(\frac{\Delta d}{d}\right) v_w$$

where $\triangle v_w$ is the relative variation of water volume concentration and $\triangle d$ is the standard deviations of *d*. In order to reduce the effect on the results of any error in the sample thickness, thicker samples are preferred.

THz biological imaging was originally introduced in 1995 by Hu and Nuss in relation to terahertz time-domain spectroscopy [103]. A fresh leaf (the sample) was scanned using a two-dimensional motion stage and the transmitted intensities were acquired and processed in real time. The spectral information at each pixel was obtained and processed, using a commercial signal processing board (Data Translation DT3818) in less than 5 ms. The amplitude and phase of the THz waveforms were extracted by a previously proposed speech recognition algorithm [104]. The water distribution inside a fresh leaf was estimated over 48 h. The results involved the capture of 30,000 pixels at a rate of 12 pixels/s with roughly 400 μm resolution. In 2000, time-domain transmission imaging using THz pulses was demonstrated at the higher frequency of 10 THz by Cho *et al.* [105], permitting imaging of cells in an onion membrane with approximately 50 μm resolution. The result clearly indicated the different water content of the cells and the intercellular regions. Cole *et al.* demonstrated *in vivo* measurements of skin in 2001 [106]. It was shown that THz pulsed imaging in reflection geometry setup could measure the changes in skin hydration due to absorption. Additionally, using the system, they could differentiate between skin tissue and related cancers (basal cell carcinoma), both *in vitro* and *in vivo*, by examining the pulse shape [24,107]. In 2003, David *et al.* [108] obtained 3-D information from dental tissue using TPI in reflective mode. The thickness of the enamel at each of the artificially induced steps were measured accurately within 10 μm of the expected values. In 2004, a finite difference time domain (FDTD) model [109,110] was applied to accurately simulate the interaction of THz radiation with water and this was successfully used to analyse experimental skin cancer data. The interaction of THz radiation with normal human skin on the forearms and palms of the hands (*in vivo*) of 20 volunteers, were compared. It was shown that the thickness of the stratum corneum (outermost layer of skin) could be quantified by analyzing the reflected THz signal.

TPI was used in a clinical setting to image Basal cell carcinoma ex *vivo* and in *vivo* by Vincent et al. in 2004 [111,112]. The system had a usable frequency range of 0.1–3 THz with an average power of approximately 100 nW. Sweeping the optical delay through the entire THz pulse at a rate of 15 Hz, the time-domain THz waveforms were obtained. The difference between basal cell carcinoma and normal tissue, determined by TPI, has been shown to have the potential to delineate tumor edges. The diseased tissue had differentiable THz properties compared with those of normal tissue which manifested itself as a

broadening of the reflected THz pulse.

Breast cancer is one of the most commonly occurring diseases among women. As a result of technological advances in early breast cancer detection, segmental mastectomy is increasingly common, limiting total breast removal rate. However, the precision in accurately delineated tumor margins remains weak leading to second surgery. In fact, following histopathologic examination of excised tissues, up to 20% of patients are shown to have tumor at the margins [113,114]. THz phase imaging can be used to investigate the potential of breast tissue diagnosis. Fitzgerald *et al.* were the first to study the feasibility of THz pulsed imaging to map the breast tumor margins in 2003 [115]. THz phase imaging has been demonstrated to have potential to aid in the accurate identification of the locations and the removal of breast cancer intra-operatively by studying the *ex vivo* breast cancer [116,117]. In 2009, Philip *et al.* measured the complex refractive index and absorption coefficient spectra of freshly excised healthy breast tissue and breast cancer tissue from 20 breast cancer patients using transmission and reflection geometries of TPI [118].

Cartilage thickness measurement is demonstrated to be crucial when diagnosing osteoarthritis, the early symptoms of osteoarthritis. This was measured in rabbit femoral condyle by Wai et al. in 2010 [119]. Subsequently, brain cancer [120], liver cancer [121] and cervical cancer [122] have all been investigated using TPI technology. In 2015, CW in-line TDH was reported to diagnose human hepatocellular carcinoma tissue. The amplitude and phase image of samples of size 3.2 mm by 2.3 mm and 30 μm-thick, was obtained [76]. The authors demonstrated the potential of CW THz holographic imaging to diagnose early stage cancer by analyzing the reconstructed phase distribution.

In 2017, the natural dehydration process in three type of biological tissues, i.e. cattle, mutton, and pork, were investigated using a THz digital holographic system at 0.56 THz [41]. The beef slices were 1.462 mm and 1.312 mm thick; the mutton slices thicknesses 1.150 mm and 1.220 mm, and the pork slices thicknesses were 1.998 mm and 1.602 mm thick. The amplitude and absorbance images of each specimen, measured with dehydration time of 0, 40 min, 80 min, 120 min, 160 min and 1 day, were presented respectively. The results show that adipose tissues have higher transmittances to THz waves than muscle tissues in these specimens. Therefore, there are lower water content of adipose tissues than muscle tissues in different animals. In 2018, the responses of freshly excised breast tissue through 16 different samples in the 300 GHz–600 GHz have investigated using a THz-TDS system situated in a hospital [123]. They obtained complex refractive indices over 300, 400, 500 and 600 GHz wave measured. The contrast between tissue types were examined in the different frequency images. This strongly suggests that the dielectric response could potentially provide contrast for breast tissue recognition over the 300–600 GHz range.

5. Conclusion and outlook

Extensive research has been carried out to investigate THz phase imaging systems and to study their biomedical applications in recent years. We concentrate on continuous wave terahertz phase imaging. This paper provides a brief review of the methodologies employed to capture and process THz phase images. At the start of this paper, the state of THz technology is introduced. The brief review of the existing pulsed and CW THz system is discussed. THz pulsed imaging systems and methods are discussed. Following this, CW terahertz interferometric imaging is described including different holographic interferometry systems, e.g. Mach-Zehnder, Michelson and Fabry-Perot interferometers. Some methods to enhance CW THz image resolution and reconstruction are presented. Finally, some significant biomedical applications of THz phase imaging are briefly discussed.

Several bottlenecks exist in the development of terahertz phase imaging. Longer wavelength terahertz radiation exhibits strong penetration, but the sources only provide lower output power. Optical terahertz sources (shorter wavelengths) provide high output power but the radiation is more weakly penetrating. Two examples of such sources and their drawbacks are QCL, which operate at low temperatures, and optical pump THz lasers whose output power is unstable. Challenges also exist in the development of terahertz array detectors with high sensitivity, large dynamic range and large number of pixels remains a challenge. The lack of suitable beam shaping components to control the profile of the object illumination beam affects image quality. The lack of terahertz imaging lenses with large numerical aperture makes it difficult to collect high-frequency components and thus reduces resolution. Therefore, it is necessary to further develop high-performance terahertz sources, detectors and imaging devices, which are the foundation and prerequisite for future work.

Two interrelated directions of future development will involve the application in the THZ regime of the modern super-resolution techniques of computational imaging [124] and artificial intelligence [125]. The study of material properties across the THZ range material characterization, biomedical imaging, non-destructive testing, cultural relic protection, etc. Further work will allow the establishment of the relationship between phase information and object morphology or internal structure.

The work reported here represents only a small selection of recent THz phase imaging studies and advances. There are many more THz imaging approaches like near field [126–128], computed tomography [129–131] and optical coherent tomography [132,133]. THz imaging is a truly interdisciplinary area of research and is still only in its early stages of development. Common use of any of the many systems described will depend on the price and robustness of THz imaging equipment. To reduce the costs and expand the range of applications of THz technology, will require close cooperation and collaboration of physicists, biologist, engineers and medics.

Acknowledgment

MW was supported by the H2020 ITN CELTA under grant number 675683. JTS thanks Science Foundation Ireland and Enterprise Ireland for support under the National Development Plan.

Appendix A. Supplementary material

Supplementary data to this article can be found online at https://doi.org/10.1016/j.optlastec.2019.105859.

References

[1] E. Bründermann, H.-W. Hübers, M.F. Kimmitt, Terahertz Techniques, Springer, 2012.
[2] Y.S. Lee, Principles of Terahertz science and technology, Springer Science & Business Media, 2009.
[3] C. Sirtori, Bridge for the terahertz gap, Nature 417 (2002) 132–133.
[4] B.S. Williams, Terahertz quantum-cascade lasers, Nature Photon. 1 (2017) 517–525.
[5] M.Y. Wong, G.D. Sims, I.M. Stephenson, Operation of the backward-wave oscillator, Nature 188 (1960) 803–804.
[6] S.G. Pavlov, H.-W. Hübers, H. Riemann, R.K. Zhukavin, E.E. Orlova, V.N. Shastin, Terahertz optically pumped Si: Sb laser, J. Appl. Phys. 92 (10) (2002) 5632–5634.
[7] J.R. Demers, R.T. Logan, E.R. Brown, An optically integrated coherent frequency-domain THz spectrometer with signal-to-noise ratio up to 80 dB, Microwave Photon. (2007) 92–95.
[8] S. Preu, G.H. Döhler, S. Malzer, L.J. Wang, A.C. Gossard, Tunable, continuous-wave terahertz photomixer sources and applications, J. Appl. Phys. 109 (2011) 061301.
[9] J.L. Coutaz, F. Garet, V.P. Wallace, Principles of Terahertz time-domain spectroscopy: an introductory textbook, CRC Press, 2018.
[10] M. van Exter, C. Fattinger, D. Grischkowsky, Terahertz time-domain spectroscopy of water vapor, Opt. Lett. 14 (1989) 1128–1130.
[11] Q. Wu, X.C. Zhang, Free-space electro-optic sampling of terahertz beams, Appl. Phys. Lett. 67 (1995) 3523.
[12] A. Nahata, A.S. Weling, T.F. Heinz, A wideband coherent terahertz spectroscopy system using optical rectification and electro-optic sampling, Appl. Phys. Lett. 69 (1996) 2321.
[13] (Retrieved 07/07/19). < http://www.tydexoptics.com/pdf/Golay_Detectors.pdf > .

[14] R.K. Bhan, R.S. Saxena, C.R. Jalwania, S.K. Lomash, Uncooled infrared microbolometer arrays and their characterisation techniques, Defence Sci. J. 59 (6) (2009) 580–589.

[15] D.T. Nguyen, F. Simoens, J.L. Ouvrier-Buffet, J. Meilhan, J.L. Coutaz, Broadband THz uncooled antenna-coupled microbolometer array—electromagnetic design, simulations and measurements, IEEE Trans. Terahertz Sci. Technol. 2 (3) (2012) 299–305.

[16] M. Fujiwara, T. Hirao, M. Kawada, H. Shibai, S. Matsuura, H. Kaneda, M. Patrashin, T. Nakagawa, Development of a gallium-doped germanium far-infrared photoconductor direct hybrid two-dimensional array, Appl. Opt. 42 (12) (2003) 2166–2173.

[17] (Retrieved 07/07/19). https://www.ophiropt.com/laser–measurement/sites/default/files/Pyrocam_1.pdf.

[18] S. Wang, X. Zhang, Pulsed terahertz tomography, J. Phys. D: Appl. Phys. 37 (4) (2004) R1.

[19] B. Ferguson, S. Wang, D. Gray, D. Abbot, X. Zhang, T-ray computed tomography, Opt. Lett. 27 (15) (2002) 1312–1314.

[20] S. Hunsche, M. Koch, I. Brener, M.C. Nuss, THz near-field imaging, Opt. Comm. 150 (1–6) (1998) 22–26.

[21] H. Zhong, A. Redo-Sanchez, X. Zhang, Identification and classification of chemicals using terahertz reflective spectroscopic focal-plane imaging system, Opt. Express 14 (20) (2006) 9130–9141.

[22] L. Zhang, H. Zhong, Y. Zhang, N. Karpowicz, C. Zhang, Y. Zhao, X. Zhang, Terahertz wave focal-plane multiwavelength phase imaging, JOSA A 26 (5) (2009) 1187–1190.

[23] S.W. Smye, J.M. Chamberlain, A.J. Fitzgerald, E. Berry, The interaction between Terahertz radiation and biological tissue, Phys. Med. Biol. 46 (2001) R101–R102.

[24] E. Pickwell, V.P. Wallace, B.E. Cole, S. Ali, C. Longbottom, R.J. Lynch, M. Pepper, A comparison of terahertz pulsed imaging with transmission microradiography for depth measurement of enamel demineralisation in vitro, Caries Res. 41 (1) (2007) 49–55.

[25] R.M. Woodward, B.E. Cole, V.P. Wallace, R.J. Pye, D.D. Arnone, E.H. Linfield, M. Pepper, Terahertz pulse imaging in reflection geometry of human skin cancer and skin tissue, Phys. Med. Biol. 47 (21) (2002) 3853.

[26] Z.D. Taylor, R.S. Singh, M.O. Culjat, J.Y. Suen, W.S. Grundfest, H. Lee, E.R. Brown, Reflective terahertz imaging of porcine skin burns, Opt. Lett. 33 (11) (2008) 1258–1260.

[27] Q. Wu, T.D. Hewitt, X. Zhang, Two-dimensional electro-optic imaging of THz beams, Appl. Phys. Lett. 69 (8) (1996) 1026–1028.

[28] M. Servin, J.L. Marroquin, D. Malacara, F.J. Cuevas, Phase unwrapping with a regularized phase-tracking system, Appl. Opt. 37 (10) (1998) 1917–1923.

[29] M. Servin, F.J. Cuevas, D. Malacara, J.L. Marroquin, R. Rodriguez-Vera, Phase unwrapping through demodulation by use of the regularized phase-tracking technique, Appl. Opt. 38 (10) (1999) 1934–1941.

[30] L. Zhang, Y. Zhang, C. Zhang, Y. Zhao, X. Liu, Terahertz multiwavelength phase imaging without 2π ambiguity, Opt. Lett. 31 (2006) 3668–3670.

[31] A. Boh Ruffin, T. Norris, J. Whitaker, L. Sanchez-Palcenia, L. Le Hors, Time reversal and object reconstruction using single-cycle terahertz pulses, Opt. Photon. News 11 (2000) 40.

[32] Y. Zhang, W. Zhou, X. Wang, Y. Cui, W. Sun, Terahertz digital holography, Strain 44 (5) (2008) 380–385.

[33] X. Wang, W. Xiong, W. Sun, W. Zhang, Coaxial waveguide mode reconstruction and analysis with THz digital holography, Opt. Express 20 (7) (2012) 7706–7715.

[34] S. Feng, H.G. Winful, R.W. Hellwarth, Gouy shift and temporal reshaping of focused single-cycle electromagnetic pulses, Opt. Lett. 23 (5) (1998) 385–387.

[35] S. Feng, H.G. Winful, Physical origin of the Gouy phase shift, Opt. Lett. 26 (8) (2001) 485–487.

[36] X. Wang, W. Sun, Y. Cui, J. Ye, S. Feng, Y. Zhang, Complete presentation of the Gouy phase shift with the THz digital holography, Opt. Express 21 (2) (2013) 2337–2346.

[37] A. Minasyan, C. Trovato, J. Degert, E. Freysz, E. Brasselet, E. Abraham, Geometric phase shaping of terahertz vortex beams, Optics Lett. 42 (1) (2017) 41–44.

[38] X. Wang, J. Shi, W. Sun, S. Feng, P. Han, J. Ye, Y. Zhang, Longitudinal field characterization of converging terahertz vortices with linear and circular polarizations, Opt. Express 24 (7) (2016) 7178–7190.

[39] D. Hu, X. Wang, S. Feng, J. Ye, W. Sun, Q. Kan, P.J. Klar, Y. Zhang, Ultrathin terahertz planar elements, Adv. Opt. Mater 1 (2) (2013) 186–191.

[40] Z. Wu, X. Wang, W. Sun, S. Feng, P. Han, J. Ye, Y. Zhang, Vector characterization of zero-order terahertz Bessel beams with linear and circular polarizations, Sci. Rep. 7 (1) (2017) 13929.

[41] L. Guo, X. Wang, P. Han, W. Sun, S. Feng, J. Ye, Y. Zhang, Observation of dehydration dynamics in biological tissues with terahertz digital holography, App. Optics 56 (13) (2017) F173–F178.

[42] F. Kaori, *T*Hz pulsed time-domain imaging (THz pulsed TDI), THz Technology Applied to Cultural Heritage in Practice, Springer, 2016, pp. 47–65.

[43] J. Darmo, V. Tamosiunas, G. Fasching, J. Kröll, K. Unterrainer, M. Beck, M. Giovannini, J. Faist, C. Kremser, P. Debbage, Imaging with a Terahertz quantum cascade laser, Opt. Express 12 (9) (2004) 1879–1884.

[44] A.W. Lee, Q. Qin, S. Kumar, B.S. Williams, Q. Hu, J.L. Reno, Real-time terahertz imaging over a standoff distance (> 25 meters), Appl. Phys. Lett. 89 (14) (2006) 141125.

[45] S. Ariyoshi, C. Otani, A. Dobroiu, H. Sato, K. Kawase, H.M. Shimizu, T. Taino, H. Matsuo, Terahertz imaging with a direct detector based on superconducting tunnel junctions, Appl. Phys. Lett. 88 (20) (2006) 203503.

[46] B.N. Behnken, G. Karunasiri, D.R. Chamberlin, P.R. Robrish, J. Faist, Real-time imaging using a 2.8 THz quantum cascade laser and uncooled infrared microbolometer camera, Opt. Lett. 33 (5) (2008) 440–442.

[47] D. Gabor, A new microscopic principle, Nature 161 (1948) 777–778.

[48] U. Schnars, W. Jüptner, Direct recording of holograms by a CCD target and numerical reconstruction, Appl. Opt. 33 (2) (1994) 179–181.

[49] J.W. Goodman, Introduction to fourier optics, third Ed., Roberts and company publishers, 2005.

[50] L. Rong, T. Latychevskaia, D. Wang, X. Zhou, H. Huang, Z. Li, Y. Wang, Terahertz in-line digital holography of dragonfly hindwing: amplitude and phase reconstruction at enhanced resolution by extrapolation, Opt. Express 22 (2014) 17236–17245.

[51] K. Xue, Q. Li, Y. Li, Q. Wang, Continuous-wave terahertz in-line digital holography, Opt. Lett. 37 (2012) 3228–3230.

[52] P. Zolliker, E. Hack, THz holography in reflection using a high resolution microbolometer array, Opt. Express 23 (2015) 10957–10967.

[53] S. Ding, Q. Li, Y. Li, Q. Wang, Continuous-wave terahertz digital holography by use of a pyroelectric array camera, Opt. Lett. 36 (2011) 1993–1995.

[54] M. Wan, D. Wang, L. Rong, Y. Wang, H. Huang, B. Li, Continuous-wave terahertz reflective off-axis digital holography, Proc. SPIE 10157 (2016) 101571U.

[55] R.J. Mahon, J.A. Murphy, W. Lanigan, Digital holography at millimeter wavelengths, Opt. Commun. 260 (2) (2006) 469–473.

[56] V.S. Cherkassky, B.A. Knyazev, S.V. Kozlov, V.V. Kubarev, G.N. Kulipanov, A.N. Matveenko, V.M. Popik, D.N. Root, P.D. Rudych, O.A. Shevchenko, A.V. Trifutina, Terahertz imaging and holography with a high-power free electron laser, IRMMW-THz 2005 (2) (2005) 337–338.

[57] B.A. Knyazev, A.L. Balandin, V.S. Cherkassky, Y.Y. Choporova, V.V. Gerasimov, M.A. Dem'yanenko, D.G. Esaev, A.A. Nikitin, V.V. Pickalov, M.G. Vlasenko, D.G. Rodionov, O.A. Shevchenko, Classic holography, tomography and speckle metrology using a high-power terahertz free electron laser and real-time image detectors, IRMMW-THz 2010 (2010) 1–3.

[58] A. Enayati, A. Tamminen, J. Ala-Laurinaho, A.V. Räisänen, G.A. Vandenbosch, W. De Raedt, THz holographic imaging: a spatial-domain technique for phase retrieval and image reconstruction, Microwave Symposium Digest (MTT), 2012 IEEE MTT-S International, 2012, pp. 1–3.

[59] E. Hack, P. Zolliker, Terahertz holography for imaging amplitude and phase objects, Opt. Express 22 (2014) 16079–16086.

[60] M.S. Heimbeck, W.R. Ng, D.R. Golish, M.E. Gehm, H.O. Everitt, Terahertz digital holographic imaging of voids within visibly opaque dielectrics, IEEE Trans. Terahertz Sci. Technol. 5 (1) (2015) 110–116.

[61] (Retrieved 07/07/19). https://www.vadiodes.com/en/.

[62] E. Hack, L. Valzania, G. Gäumann, M. Shalaby, C.P. Hauri, P. Zolliker, Comparison of thermal detector arrays for off-axis THz holography and real-time THz imaging, Sensors 16 (2) (2016) 221.

[63] L. Valzania, P. Zolliker, E. Hack, Topography of hidden objects using THz digital holography with multi-beam interferences, Opt. Express 25 (2017) 11038–11047.

[64] M. Yamagiwa, T. Ogawa, T. Minamikawa, H. Yamamoto, T. Yasui, Off-axis digital holography in THz region, Digital Holography and Three-Dimensional Imaging, Optical Society of America, 2017, p. M3A-5.

[65] Q. Li, K. Xue, Y. Li, Q. Wang, Experimental research on terahertz Gabor inline digital holography of concealed objects, Appl. Opt. 51 (2012) 7052–7058.

[66] Q. Li, S.H. Ding, Y.D. Li, K. Xue, Q. Wang, Experimental research on resolution improvement in CW THz digital holography, Appl. Phys. B. 107 (1) (2012) 103–110.

[67] Q. Li, S.H. Ding, Y.D. Li, K. Xue, Q. Wang, Research on reconstruction algorithms in 2.52 THz off–axis digital holography, J. Infrared Millim. Terahertz Waves 33 (10) (2012) 1039–1051.

[68] J. Hu, Q. Li, S. Cui, Research on object-plane constraints and hologram expansion in phase retrieval algorithms for continuous-wave terahertz inline digital holography reconstruction, Appl. Opt. 53 (2014) 7112–7119.

[69] H. Huang, D. Wang, L. Rong, X. Zhou, Z. Li, Y. Wang, Application of autofocusing methods in continuous-wave terahertz in-line digital holography, Opt. Commun. 346 (2015) 93–98.

[70] H. Huang, D. Wang, W. Li, L. Rong, Z.D. Taylor, Q. Deng, B. Li, Y. Wang, W. Wu, S. Panezai, Continuous-wave terahertz multi-plane in-line digital holography, Opt. Lasers Eng. 94 (2017) 76–81.

[71] F. Le Clerc, M. Gross, L. Collot, Synthetic-aperture experiment in the visible with on-axis digital heterodyne holography, Opt. Lett. 26 (2001) 1550–1552.

[72] J.H. Massig, Digital off-axis holography with a synthetic aperture, Opt. Lett. 27 (2002) 2179–2181.

[73] T. Gutzler, T.R. Hillman, S.A. Alexandrov, D.D. Sampson, Coherent aperture-synthesis, wide-field, high-resolution holographic microscopy of biological tissue, Opt. Lett. 35 (2010) 1136–1138.

[74] H. Huang, L. Rong, D. Wang, W. Li, Q. Deng, B. Li, Y. Wang, Z. Zhan, X. Wang, W. Wu, Synthetic aperture in terahertz in-line digital holography for resolution enhancement, Appl. Opt. 55 (2016) A43–A48.

[75] D. Wang, Y. Zhao, L. Rong, M. Wan, X. Shi, Y. Wang, J.T. Sheridan, Expanding the field-of-view and profile measurement of covered objects in continuous-wave terahertz reflective digital holography, Opt. Eng. 58 (2) (2019) 023111.

[76] L. Rong, T. Latychevskaia, C. Chen, D. Wang, Z. Yu, X. Zhou, Z. Li, H. Huang, Y. Wang, Z. Zhou, Terahertz in-line digital holography of human hepatocellular carcinoma tissue, Sci. Rep. 5 (1) (2015) 8445.

[77] T. Latychevskaia, H.-W. Fink, Resolution enhancement in digital holography by self-extrapolation of holograms, Opt. Express 21 (6) (2013) 7726–7733.

[78] M.S. Heimbeck, M.K. Kim, D.A. Gregory, H.O. Everitt, Terahertz digital holography using angular spectrum and dual wavelength reconstruction methods, Opt. Express 19 (2011) 9192–9200.

[79] J. Gass, A. Dakoff, M.K. Kim, Phase imaging without 2π ambiguity by

multiwavelength digital holography, Opt. Lett. 28 (13) (2003) 1141–1143.
[80] M. Suga, Y. Sasaki, T. Sasahara, T. Yuasa, C. Otani, THz phase-contrast computed tomography based on Mach-Zehnder interferometer using continuous wave source: proof of the concept, Opt. Express 21 (2013) 25389–25402.
[81] M. Locatelli, M. Ravaro, S. Bartalini, L. Consolino, M.S. Vitiello, R. Cicchi, F. Pavone, P. De Natale, Real-time terahertz digital holography with a quantum cascade laser, Sci. Rep. 5 (1) (2015) 13566.
[82] X. Wang, L. Hou, Y. Zhang, Continuous-wave terahertz interferometry with multiwavelength phase unwrapping, Appl. Opt. 49 (2010) 5095–5102.
[83] Y. Wang, Z. Zhao, Z. Chen, L. Zhang, K. Kang, J. Deng, Continuous-wave terahertz phase imaging using a far-infrared laser interferometer, Appl. Opt. 50 (2011) 6452–6460.
[84] K. Yatabe, K. Ishikawa, Y. Oikawa, Simple, flexible, and accurate phase retrieval method for generalized phase-shifting interferometry, J. Opt. Soc. Am. A 34 (2017) 87–96.
[85] W. Sun, X. Wang, Y. Zhang, Continuous wave terahertz phase imaging with three-step phase-shifting, Optik 124 (22) (2013) 5533–5536.
[86] J. Lu, C. Kuo, C. Chiu, H. Chen, Y. Hwang, C. Pan, C. Sun, THz interferometric imaging using subwavelength plastic fiber-based THz endoscopes, Opt. Express 16 (2008) 2494–2501.
[87] J. Lu, C. Chiu, C. Kuo, C. Lai, H. Chang, Y. Hwang, C. Pan, C. Sun, Terahertz scanning imaging with a subwavelength plastic fiber, Appl. Phys. Lett. 92 (2008) 084102.
[88] K. Giewekemeyer, P. Thibault, S. Kalbfleisch, A. Beerlink, C.M. Kewish, M. Dierolf, F. Pfeiffer, T. Salditt, Quantitative biological imaging by ptychographic x-ray diffraction microscopy, PNAS 107 (2) (2010) 529–534.
[89] S. Sala, D.J. Batey, A. Prakash, S. Ahmed, C. Rau, P. Thibault, Ptychographic X-ray computed tomography at a high-brilliance X-ray source, Opt. Express 27 (2019) 533–542.
[90] A.M. Maiden, J.M. Rodenburg, M.J. Humphry, Optical ptychography: a practical implementation with useful resolution, Opt. Lett. 35 (2010) 2585–2587.
[91] P. Thibault, M. Dierolf, O. Bunk, A. Menzel, F. Pfeiffer, Probe retrieval in ptychographic coherent diffractive imaging, Ultramicroscopy 109 (4) (2009) 338–343.
[92] L. Valzania, T. Feurer, P. Zolliker, E. Hack, Terahertz ptychography, Opt. Lett. 43 (2018) 543–546.
[93] A.M. Maiden, J.M. Rodenburg, An improved ptychographical phase retrieval algorithm for diffractive imaging, Ultramicroscopy 109 (10) (2009) 1256–1262.
[94] L. Rong, C. Tang, D. Wang, B. Li, F. Tan, Y. Wang, X. Shi, Probe position correction based on overlapped object wavefront cross-correlation for continuous-wave terahertz ptychography, Opt. Express 27 (2019) 938–950.
[95] L. Valzania, P. Zolliker, E. Hack, Coherent reconstruction of a textile and a hidden object with terahertz radiation, Optica 6 (2019) 518–523.
[96] Y. Sun, M.Y. Sy, Y.J. Wang, A.T. Ahuja, Y.T. Zhang, E. Pickwell-Macpherson, A promising diagnostic method: Terahertz pulsed imaging and spectroscopy, World J. Radiol. 3 (3) (2011) 55–65.
[97] C. Yu, S. Fan, Y. Sun, E. Pickwell-Macpherson, The potential of terahertz imaging for cancer diagnosis: A review of investigations to date, Quant. Imaging Med. Surg. 2 (1) (2012) 33–45.
[98] Q. Sun, Y. He, K. Liu, S. Fan, E.P. Parrott, E. Pickwell-MacPherson, Recent advances in terahertz technology for biomedical applications, Quant. Imaging Med. Surg. 7 (3) (2017) 345–355.
[99] Y.K. Lee, S.W. Choi, S.T. Han, D.H. Woo, H.S. Chun, Detection of foreign bodies in foods using continuous wave terahertz imaging, J. Food Prot. 75 (1) (2012) 179–183.
[100] G. Ok, K. Park, H.J. Kim, H.S. Chun, S.W. Choi, High-speed terahertz imaging toward food quality inspection, Appl. Opt. 53 (2014) 1406–1412.
[101] G. Ok, H.J. Kim, H.S. Chun, S.W. Choi, Foreign-body detection in dry food using continuous sub-terahertz wave imaging, Food Control 42 (2014) 284–289.
[102] Y. Wang, H. Minamide, M. Tang, T. Notake, H. Ito, Study of water concentration measurement in thin tissues with terahertz-wave parametric source, Opt. Express 18 (2010) 15504–15512.
[103] B.B. Hu, M.C. Nuss, Imaging with terahertz waves, Opt. Lett. 20 (1995) 1716–1718.
[104] J. Picone, Fundamentals of speech recognition: A short course, Institute for Signal and Information Processing, Mississippi State University, 1996.
[105] P.Y. Han, G.C. Cho, X.-C. Zhang, Time-domain transillumination of biological tissues with terahertz pulses, Opt. Lett. 25 (2000) 242–244.
[106] B.E. Cole, R.M. Woodward, D.A. Crawley, V.P. Wallace, D.D. Arnone, M. Pepper, Terahertz imaging and spectroscopy of human skin in vivo, Proc. SPIE 4276 (2001) 1–11.
[107] E. Pickwell, B.E. Cole, A.J. Fitzgerald, M. Pepper, V.P. Wallace, In vivo study of human skin using pulsed terahertz radiation, Phys. Med. Biol. 49 (9) (2004) 1595–1607.
[108] D.A. Crawley, C. Longbottom, V.P. Wallace, B.E. Cole, D.D. Arnone, M. Pepper, Three-dimensional terahertz pulse imaging of dental tissue, J. Biomed. Opt. 8 (2) (2003) 303–308.
[109] E. Pickwell, B.E. Cole, A.J. Fitzgerald, V.P. Wallace, M. Pepper, Simulation of terahertz pulse propagation in biological systems, Appl. Phys. Lett. 84 (12) (2004) 2190–2192.
[110] E. Pickwell, A.J. Fitzgerald, B.E. Cole, P.F. Taday, R.J. Pye, T. Ha, M. Pepper, V.P. Wallace, Simulating the response of terahertz radiation to basal cell carcinoma using ex-vivo spectroscopy measurements, J. Biomed Opt. 10 (6) (2005) 064021.
[111] V.P. Wallace, P.F. Taday, A.J. Fitzgerald, R.M. Woodward, J. Cluff, R.J. Pye, D.D. Arnone, Terahertz pulsed imaging and spectroscopy for biomedical and pharmaceutical applications, Faraday Discuss. 126 (2004) 255–263.
[112] V.P. Wallace, A.J. Fitzgerald, S. Shankar, N. Flanagan, R. Pye, J. Cluff, D.D. Arnone, Terahertz pulsed imaging of basal cell carcinoma ex vivo and in vivo, Br. J. Dermatol. 151 (2) (2004) 424–432.
[113] J. Landercasper, E. Whitacre, A.C. Degnim, M. Al-Hamadani, Reasons for re-excision after lumpectomy for breast cancer: insight from the American Society of Breast Surgeons Mastery (SM) database, Ann. Surg. Oncol. 21 (10) (2014) 3185–3191.
[114] R. Jeevan, D.A. Cromwell, M. Trivella, G. Lawrence, O. Kearins, J. Pereira, C. Sheppard, C.M. Caddy, J.H.P. van der Meulen, Reoperation rates after breast conserving surgery for breast cancer among women in England: retrospective study of hospital episode statistics, BMJ 345 (2012) e4505 jul12 2.
[115] P.J. Bolan, S. Meisamy, E.H. Baker, J. Lin, T. Emory, M. Nelson, L.I. Everson, D. Yee, M. Garwood, In vivo quantification of choline compounds in the breast with 1H MR spectroscopy, Magn. Reson. Med. 50 (6) (2003) 1134–1143.
[116] A.J. Fitzgerald, V.P. Wallace, M. Jimenez-Linan, L. Bobrow, R.J. Pye, A.D. Purushotham, D.D. Arnone, Terahertz pulsed imaging of human breast tumors, Radiology 239 (2) (2006) 533–540.
[117] F. Wu, Z.B. Wang, Y.D. Cao, W.Z. Chen, J. Bai, J.Z. Zou, H. Zhu, A randomised clinical trial of high-intensity focused ultrasound ablation for the treatment of patients with localised breast cancer, Br. J. Cancer. 89 (12) (2003) 2227–2233.
[118] P.C. Ashworth, E. Pickwell-MacPherson, E. Provenzano, S.E. Pinder, A.D. Purushotham, M. Pepper, V.P. Wallace, Terahertz pulsed spectroscopy of freshly excised human breast cancer, Opt. Express 17 (15) (2009) 12444–12454.
[119] W. Kan, W. Lee, W. Cheung, V.P. Wallace, E. Pickwell-MacPherson, Terahertz pulsed imaging of knee cartilage, Biomed. Opt. Exp. 1 (3) (2010) 967–974.
[120] S.J. Oh, S. Kim, Y.B. Ji, K. Jeong, Y. Park, J. Yang, D.W. Park, S.K. Noh, S. Kang, Y. Huh, J. Son, J. Suh, Study of freshly excised brain tissues using terahertz imaging, Biomed. Opt. Exp. 5 (8) (2014) 2837–2842.
[121] C.H. Zhang, G.F. Zhao, B.B. Jin, Y.Y. Hou, H.H. Jia, J. Chen, P.H. Wu, Terahertz imaging on subcutaneous tissues and liver inflamed by liver cancer cells, Terahertz Sci. Technol. 5 (3) (2012) 114–123.
[122] E. Jung, M. Lim, K. Moon, Y. Do, S. Lee, H. Han, H. Choi, K. Sik Cho, K. Kim, Terahertz pulse Imaging of micro-metastatic lymph nodes in early-stage cervical cancer patients, J. Opt. Soc. Korea 15 (2) (2011) 155–160.
[123] Q. Cassar, A. Al-Ibadi, L. Mavarani, P. Hillger, J. Grzyb, G. MacGrogan, T. Zimmer, U.R. Pfeiffer, J. Guillet, P. Mounaix, Pilot study of freshly excised breast tissue response in the 300–600 GHz range, Biomed. Opt. Exp. 9 (7) (2018) 2930–2942.
[124] J.N. Mait, G.W. Euliss, R.A. Athale, Computational imaging, Adv. Opt. Photon. 10 (2018) 409–483.
[125] G. Barbastathis, A. Ozcan, G. Situ, On the use of deep learning for computational imaging, Optica 6 (2019) 921–943.
[126] C.G. Wade, N. Šibalić, N.R. de Melo, J.M. Kondo, C.S. Adams, K.J. Weatherill, Real-time near-field terahertz imaging with atomic optical fluorescence, Nat. Photon. 11 (2017) 40–43.
[127] R.I. Stantchev, B. Sun, S.M. Hornett, P.A. Hobson, G.M. Gibson, M.J. Padgett, E. Hendry, Noninvasive, near-field terahertz imaging of hidden objects using a single-pixel detector, Sci. Adv. 2 (6) (2016) e1600190.
[128] S. Chen, L. Du, K. Meng, J. Li, Z. Zhai, Q. Shi, Z. Li, L. Zhu, Terahertz wave near-field compressive imaging with a spatial resolution of over λ/100, Opt. Lett. 44 (2019) 21–24.
[129] D. Wang, B. Li, L. Rong, Z. Xu, Y. Zhao, J. Zhao, Y. Wang, C. Zhai, Extended depth of field in continuous-wave terahertz computed tomography based on Bessel beam, Opt. Commun. 432 (1) (2019) 20–26.
[130] B. Li, D. Wang, L. Rong, C. Zhai, Y. Wang, J. Zhao, Application of continuous-wave terahertz computed tomography for the analysis of chicken bone structure, Opt. Eng. 57 (2) (2018) 023105.
[131] J.P. Guillet, B. Recur, L. Frederique, B. Bousquet, L. Canioni, I. Manek-Hönninger, P. Desbarats, P. Mounaix, Review of terahertz tomography techniques, J Infrared Milli Terahz Waves 35 (2014) 382–411.
[132] T. Nagatsuma, H. Nishii, T. Ikeo, Terahertz imaging based on optical coherence tomography, Photon. Res. 2 (2014) B64–B69.
[133] C.L.K. Dandolo, M. Lopez, K. Fukunaga, Y. Ueno, R. Pillay, D. Giovannacci, Y.L. Du, X. Bai, M. Menu, V. Detalle, "Toward a multimodal fusion of layered cultural object images: complementarity of optical coherence tomography and terahertz time-domain imaging in the heritage field", Appl. Opt. 58 (2019) 1281–1290.